Cerebral Cortex September 2011;21:2003–2013
doi:10.1093/cercor/bhq268
Advance Access publication January 31, 2011

Association between Functional Connectivity Hubs and Brain Networks

Dardo Tomasi[1] and Nora D. Volkow[1,2]

[1]National Institute on Alcohol Abuse and Alcoholism, Bethesda, MD 20892, USA and [2]National Institute on Drug Abuse, Bethesda, MD 20892, USA

Address correspondence to Dr Dardo Tomasi, Laboratory of Neuroimaging (LNI/NIAAA), Medical Department, Building 490, Brookhaven National Laboratory, 30 Bell Avenue, Upton, NY 11973, USA. Email: tomasi@bnl.gov.

Functional networks are usually accessed with "resting-state" functional magnetic resonance imaging using preselected "seeds" regions. Frequently, however, the selection of the seed locations is arbitrary. Recently, we proposed local functional connectivity density mapping (FCDM), an ultrafast data-driven to locate highly connected brain regions (functional hubs). Here, we used the functional hubs obtained from local FCDM to determine the functional networks of the resting state in 979 healthy subjects without a priori hypotheses on seed locations. In addition, we computed the global functional connectivity hubs. Seven networks covering 80% of the gray matter volume were identified. Four major cortical hubs (ventral precuneus/posterior cingulate, inferior parietal cortex, cuneus, and postcentral gyrus) were linked to 4 cortical networks (default mode, dorsal attention, visual, and somatosensory). Three subcortical networks were associated to the major subcortical hubs (cerebellum, thalamus, and amygdala). The networks differed in their resting activity and topology. The higher coupling and overlap of subcortical networks was associated to higher contribution of short-range functional connectivity in thalamus and cerebellum. Whereas cortical local FCD hubs were also hubs of long-range connectivity, which corroborates the key role of cortical hubs in network architecture, subcortical hubs had minimal long-range connectivity. The significant variability among functional networks may underlie their sensitivity/resilience to neuropathology.

Keywords: functional connectivity, 1000 functional connectomes

Introduction

Which brain networks support the resting conscious state and how are they organized? Magnetic resonance imaging (MRI) studies assessing the functional connectivity of the human brain in resting conditions have identified large-scale brain networks that have been linked to neurodegenerative diseases (Seeley et al. 2009). Of these, the default mode network (DMN) is the most conspicuous since its activity is highest in resting conditions, whereas it decreases during goal-oriented task performance (Shulman et al. 1997).

Traditionally, the functional connectivity among brain regions is assessed using preselected regions-of-interest (ROIs) (i.e., "seeds regions") from which the time-varying blood oxygenation level–dependent MRI signals are extracted to compute their correlation with signals in other brain areas (Biswal et al. 1995). However, these methods are limited because they relay strongly on a priori selection of the location of the seed regions. Thus, the nature and number of independent networks supporting the resting state of brain function are still uncertain. A data-driven approach based on graph theory was recently proposed to assess the distribution of functional hubs in the human brain from MRI data sets (van den Heuvel et al. 2008; Buckner et al. 2009). This method is based on the computation of the number of functional connections per voxel (edges in graph theory), does not require a priori selection of seed regions, and was shown to exhibit good correspondence with structural connectivity studies that used diffusion tensor imaging (van den Heuvel et al. 2009). Prominent functional hubs were recently identified in the DMN as well as in dorsal parietal and prefrontal regions using this approach (Buckner et al. 2009). We hypothesized that in resting conditions, these hub regions would be functionally connected to minimally overlapping networks that would have different topological architecture.

We aimed to test this hypothesis in a large sample of brain images of healthy subjects from the open access image database "1000 Functional Connectomes Project" (Biswal et al. 2010). We used functional connectivity density mapping (FCDM; Tomasi and Volkow 2010), a novel ultrafast (1000 times faster) method that is sensitive to the number of local functional connections of the brain regions. Using this approach, we showed that the local functional connectivity density (*f*FCD) has a "scale-free" distribution in the brain (Tomasi and Volkow 2010), with few hubs and numerous weakly connected nodes, which is consistent with the emergence of scaling in neural networks (Barabasi and Albert 1999; Achard et al. 2006; Barabasi 2009; He et al. 2010).

Thus, armed with FCDM and the image database of the 1000 Functional Connectomes Project, we aimed to determine the properties of the resting state networks associated to the major *f*FCD hubs in cortical and subcortical brain regions. We hypothesized that the networks connected to the hubs would have minimal overlap and different scale-free topology and that the entire DMN would be connected to the main *f*FCD hub in the brain.

Materials and Methods

Subjects

We used resting-state functional connectivity data sets corresponding to 979 healthy subjects (for demographic information, see Table 1) from 19 of the research sites of the image repository 1000 Functional Connectomes Project, which can be assessed at http://www.nitrc.org/projects/fcon_1000/. Data sets from the remaining 16 sites were not included because they were not available (pending verification of institutional review board status) at the time of the study or did not meet the imaging acquisition criteria of the study (3 s $\geq$ time repetition, full brain coverage, time points > 100, spatial resolution better than 4 mm).

Functional Hub Mapping

Image preprocessing was performed with the Statistical Parameter Mapping package SPM2 (Wellcome Trust Centre for Neuroimaging). A 12-parameter affine transformation was used for realignment and for spatial normalization to the stereotactic space of the Montreal

Published by Oxford University Press 2011.

Neurological Institute (MNI). Subsequent spatial normalization was carried out with medium regularization, 16 nonlinear iterations, a voxel size of 3 × 3 × 3 mm^3, and the SPM2 EPI.mnc template. Motion-related signal fluctuations were removed from the time-varying data using multilinear regression with the 6 realignment parameters, and 0.01–0.10 Hz band-pass temporal filtering was applied to remove magnetic field drifts of the scanner (Foerster et al. 2005) and physiologic noise of high-frequency components (Cordes et al. 2001) using IDL (ITT Visual Information Solutions).

Local FCD

The Pearson linear correlation coefficient, R, was used to evaluate the strength of the functional connectivity between voxels. Functional connections with correlation coefficient, $R > 0.6$, were considered significant. The number of significant functional connections per voxel in the "local cluster," k, was computed using a 3D searching algorithm developed in IDL.

Gobal FCD

We implemented a high-resolution (3 mm isotropic) voxelwise approach based on graph theory methods to compute the total number of functional connections in gray matter, K, to contrast the *l*FCD measures with traditional measures of graph theory approaches (van den Heuvel et al. 2008; Buckner et al. 2009). For this purpose, a threshold $R > 0.6$ was used to compute K. Note that differently to the *l*FCD calculation, the computation of K was not restricted to the local cluster. Thus, this computer-demanding approach computed 4.05×10^9 paired correlations per subject and was optimally implementer in C programming language to speed up the calculation of the global FCD (*g*FCD), which in average required 3 h per subject in a 2 GHz-Xeon Windows XP platform.

To minimize the differences in the functional anatomy of the brain across subjects (Friston et al. 2007), spatial smoothing (8 mm) was applied to *l*FCD and *g*FCD maps using SPM2.

Statistical Analyses

The distribution of the *l*FCD varied across research centers, likely due to differences in acquisition parameters, instruments, demographic variables, and potential differences in resting conditions (e.g., eyes opened/closed, awake/sleep, etc.). The use of a single scaling factor for each research site, $1/k_0$, reflecting the mean *l*FCD across subjects and voxels in the brain, k_0, allowed us to normalize the distribution of the *l*FCD and merge the data sets from different research sites (Tomasi and Volkow 2010). Similarly, a single scaling factor for each research site, $1/K_0$, reflecting the mean *g*FCD across subjects and voxels in the brain, K_0, allowed us to normalize the distribution of the *g*FCD and merge the data sets from different research sites.

Table 1

Available demographic data for the selected resting-state functional MRI datasets from the image repository for the 1000 Functional Connectomes Project

Dataset	Subjects	Age (years)
Baltimore	8M/15F	20–40
Bangor	20M/0F	19–38
Beijing	76M/122F	18–26
Berlin	13M/13F	23–44
Cambridge	75M/123F	18–30
MIT	18M/20F	20–32
Cleveland	11M/20F	24–60
Dallas	12M/12F	20–71
Leiden	23M/8F	20–27
Leipzig	16M/21F	20–42
Newark	9M/10F	21–39
New York A	40M/19F	20–49
New York B	8M/12F	18–46
NYU_TRT	10M/17F	22–49
Ontario	11 subjects	N/A
Orangeburg	15M/5F	20–55
Oulu	37M/66F	20–23
Oxford	12M/10F	20–35
Queensland	11M/8F	20–34
Saint Louis	14M/17F	21–29
Taipei A	14 subjects	N/A
Taipei B	8 subjects	N/A

Network Classification

We aimed to map networks functionally connected to the functional hubs that cover at least 80% of the gray matter volume. However, the number of hubs was constrained to a minimum in order to minimize the complexity of the results. For this purpose, the most prominent *l*FCD hubs in cortical and subcortical regions were identified based on their strength (k/k_0) and their volume. Four cortical (PC-VP, Brodmann area, BA 23/31; inferior parietal cortex, BA40; cuneus, BA18; and postcentral, BA 5) and 3 subcortical (cerebellum, thalamus, and amygdala) hubs with local *l*FCD-maxima ($k/k_0 > 2$) within a spherical searching volume exceeding 20 mL were used as ROIs for subsequent seed–voxel correlation analyses (Table 2). The global component of the functional MRI (fMRI) signal fluctuations was removed from the time series to minimize global effects of heart rate and respiration. The Fisher transform was used to convert the step distributed correlation coefficients into normally distributed correlation coefficients. These rescaled correlation maps were computed, smoothed (8 mm), and uploaded into simple t-tests for group analyses of functional connectivity in SPM2, independently for each seed region. Voxels with $P < 10^{-15}$ were considered functionally connected to the hubs across subjects. The MNI coordinates of the cluster maxima were transformed to the Talairach stereotactic space using a best-fit transform (icbm_spm2tal; http://brainmap.org/icbm2tal/) that minimizes bias associated with reference frame and scaling (Lancaster et al. 2007). The brain regions were labeled according to the Talairach daemon (http://www.talairach.org/; Lancaster et al. 2000) and a query range of 5 mm to account for the spatial uncertainty of the MRI signal (Tomasi and Caparelli 2007), which results from macrovascular and susceptibility effect as well as image postprocessing steps. We further checked the labels of the hubs using the Automated Anatomical Labeling (AAL) atlas (Tzourio-Mazoyer et al. 2002) and the Brodmann atlas, which is included in the MRIcro software (http://www.cabiatl.com/mricro/).

ROI Analyses

A binary mask for each of the 7 functional connectivity networks defined above was created for the whole group of subjects. The volumes of the networks and their overlap, the average correlation strength between networks and between hubs and between hubs ad networks, and the probability distribution of the *l*FCD were evaluated within each of these 7 masks using IDL.

Results

Functional Hubs

The *l*FCD was higher for ventral than for dorsal lateral as well as for posterior than for anterior regions. The more prominent hubs (local maxima of the *l*FCD distribution) in the cortex were located in the posterior cingulate/ventral precuneus (PC-VP, BA 23/31, the global maxima of the *l*FCD), inferior

Table 2

Strength of the major functional hubs in cortical and subcortical brain regions and their location in the Talairach stereotactic space

Hub regions	X (mm)	Y (mm)	Z (mm)	*l*FCD (k/k_0)	*g*FCD (K/K_0)
PC-VP	4	−52	29	9.0	8.1
Inferior parietal	−38	−53	39	6.1	3.5
Cuneus	−24	−80	18	5.3	5.9
Postcentral	20	−44	57	4.8	3.4
Cerebellum	−9	−56	−20	4.5	1.5
Thalamus	−12	−19	8	4.0	1.4
Amygdala	24	−6	−15	2.1	2.3

parietal cortex (BA 40), cuneus (BA 18), and postcentral gyrus (BA 5; Fig. 1). The more prominent local maxima in subcortical regions were located in ventral cerebellum (declive), medial dorsal nucleus of the thalamus, and amygdala. The *l*FCD in these brain regions was 2 times higher or more than the average *l*FCD in the whole brain, and their spatial coordinates had minimal variability across research sites (7 ± 5 mm).

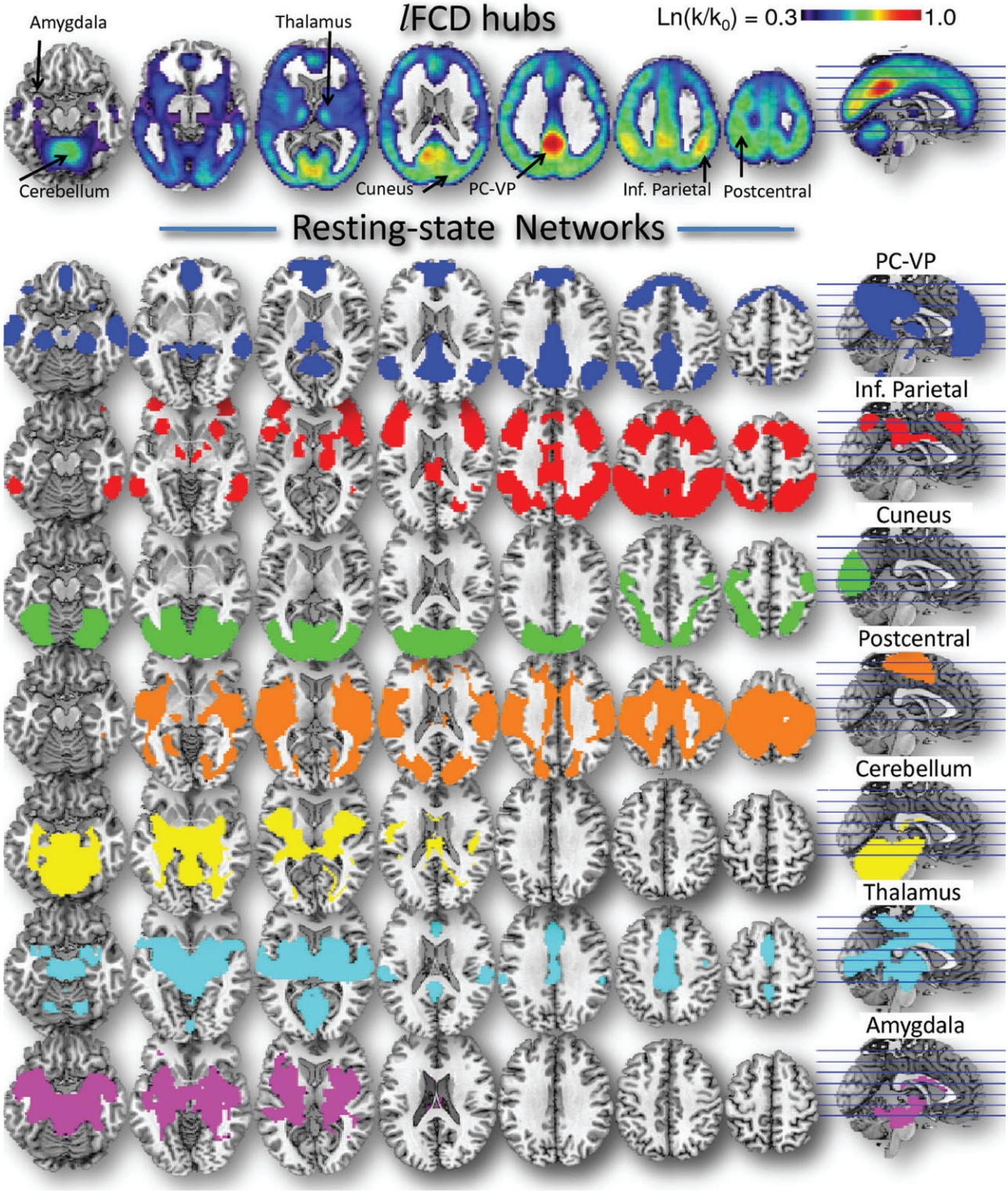

Figure 1. Resting-state Networks. Top panel: axial views showing the spatial distribution of the *l*FCD with the 7 major functional hubs (arrows) in the human brain, which reflect the average number of functional connections per voxel (*k*) across 979 subjects from 19 research sites around the world, superimposed on axial MRI views of the human brain. The FCD reaches maximal value in posterior cingulate/ventral precuneus (PC-VP; red–orange). Bottom panel: the 7 resting-state networks functionally connected to the major *l*FCD hubs were calculated using standard seed–voxel correlation analyses and *t*-tests across 979 subjects using a statistical threshold $P < 10^{-15}$.

Resting-State Hub Networks

Using standard seed–voxel correlation analyses, we identified 7 bilateral functional networks, which combined covered 80% of the gray matter volume, that were connected to the 7 cortical and subcortical hubs (Fig. 1).

The PC-VP, the strongest hub in the brain was functionally linked to regions that constitute the DMN and included ventral parietal, the angular gyrus and ventral, rostral, and orbital prefrontal cortices, as well as other limbic, temporal, and ventral visual areas, thalamus, brainstem, and the cerebellum (Table 3) and covered 17.8% of the gray matter volume. The right inferior parietal hub was functionally connected to regions that form the dorsal attention network (DAN), including dorsal parietal, temporal and prefrontal cortices, thalamus, striatum, and cerebellum, and covered 22.9% of the gray matter. The hub in the right posterior cuneus was functionally connected to a network that included occipital and parietal regions and covered 15.5% of the gray matter. The hub in the right postcentral gyrus (BA 5) was functionally connected to a network that included parietal, prefrontal, occipital, and insular cortices and covered 27.7% of the gray matter (Table 3). Figure 2A overlays these cortical hub networks on the cortical brain surface.

The hub in the right anterior lobe of the cerebellum was functionally connected to a network that covered 18.9% of the gray matter and encompassed the entire cerebellum, visual and motor cortices, limbic regions, striatum, and insula (Table 4). The hub in the right medial dorsal nucleus of the thalamus was functionally connected to a network that covered 14.5% of the gray matter and included all thalamic nuclei, limbic, parietal and prefrontal cortices, visual, auditory and motor areas, as well as cerebellum, striatum, midbrain, and pons. The hub in the left amygdala was functionally connected to a network that covered 17.1% of the gray matter and encompassed midbrain, thalamus, hippocampus, striatum, cerebellum, pons, insula, and temporal and prefrontal cortices. Figure 2*B* overlays these cortical hub networks on the cortical brain surface.

Network Overlap

The lower triangular matrix in Figure 3*A* shows the volume of the networks (main diagonal matrix elements) and the overlap between networks (off diagonal matrix elements), which was greatest for the amygdala, postcentral, and thalamus hub networks (Fig. 3*B*, connecting lines). The amygdala hub network overlapped with the cerebellum, postcentral, and thalamus hub networks. The postcentral hub network further overlapped with the thalamus, cuneus, and inferior parietal hub networks. The thalamus hub network further overlapped with the cerebellum hub network. The remaining overlaps between networks were lower than 5% of the gray matter volume.

We determined the representation of the networks in sensory areas by overlaying the networks on primary somatosensory, motor, visual, and auditory cortices (Fig. 4). Subcortical hub networks had minimal connectivity with primary somatosensory and motor cortices (BAs 1–4; Fig. 4*A*). The thalamus hub network overlapped minimally with BA 3 and more significantly with BA 2, the amygdala hub network overlapped with a small fraction of BA 3, and the cerebellum hub network overlapped minimally with BA 4. Conversely, some of the cortical hub networks had large overlap with somatosensory and motor cortices (Fig. 4*B*). The postcentral hub network overlapped largely with BAs 1–4, and the DAN overlapped largely with BA 2. Furthermore, the postcentral hub network overlapped largely with the cuneus and thalamus hub networks in the primary visual cortex (BA 17; Fig. 4*C,D*) and thalamus and amygdala hub networks in the primary auditory cortex (BA 41; Fig. 4*E,F*).

Table 3
Statistical significance (*T*-score) of clusters functionally connected to the cortical hubs (bolded) and their location in the Talairach stereotactic space

	BA/nucleus	*X* (mm)	*Y* (mm)	*Z* (mm)	*T*-score
"Default mode" network					
PC-VP	**23/31**	**4**	**−52**	**29**	**65.27**
Parahippocampal	35	−23	−22	−17	15.66
Parahippocampal	28	21	−20	−16	14.95
Angular	39	46	−61	26	37.13
Angular	39	−49	−63	25	32.9
Medial frontal	9	−1	50	23	26.08
Superior frontal	6	21	27	53	25.96
Anterior cingulate	32	−1	49	4	24.54
Middle temporal	21	55	−9	−15	24.29
Middle temporal	21	57	−32	−3	16.37
Inferior frontal	47	30	17	−15	10.69
Inferior temporal	21	−56	−11	−17	21.3
Inferior frontal	47	−28	12	−17	10.84
Superior temporal	38	−37	18	−24	9.07
Cerebellum	Semilunar lobule	−29	−74	−36	13.67
Brainstem	Medulla	−6	−48	−41	12.42
Brainstem	Medulla	5	−45	−43	11.29
Cerebellum	Pyramis	21	−78	−30	11.64
Cerebellum	Semilunar lobule	35	−68	−37	9.45
Inferior frontal gyrus	47	38	30	−8	11.06
Brainstem	Midbrain	−1	−14	−13	8.81
Brainstem	Pons	−1	−19	−22	8.34
"Dorsal attention" network					
Inferior parietal lobule	**40**	**−38**	**−53**	**39**	**52.46**
Precuneus	7	−10	−70	38	15.58
Inferior parietal lobule	40	37	−51	41	21.6
Middle frontal	9	−43	24	30	17.64
Middle frontal	10	−40	40	13	16.49
Precentral	6	−40	1	33	15.39
Middle frontal	9	43	26	32	15.04
Middle temporal	37	−54	−51	−10	14.92
Subgyral	6	−27	2	55	13.75
Precuneus	7	9	−70	41	13.6
Superior frontal	8	−4	19	49	13.38
Inferior temporal	20	52	−46	−10	13.16
Cerebellum	Pyramis	10	−72	−27	10.15
Cerebellum	Tonsil	24	−57	−33	10.11
Cerebellum	Semilunar lobule	33	−62	−42	8.75
Cerebellum	Tonsil	−29	−57	−34	9.1
Cerebellum	Pyramis	−9	−72	−30	9.05
Thalamus	Ventral lateral	10	−10	3	9
Globus pallidus	Lentiform	16	−2	7	8.78
Caudate	Body	10	6	13	8.64
Hippocampus		−26	−38	−2	8.03
"Visual" network					
Cuneus	**18**	**−24**	**−80**	**18**	**53.81**
Middle occipital	19	26	−82	19	34.05
Cuneus	18	4	−82	16	26.62
Fusiform	19	−23	−68	−11	24.91
Lingual	18	−9	−74	−6	23.75
Precentral	4	−41	−15	54	11.79
Precuneus	7	−7	−47	59	8.04
"Somatosensory" network					
Postcentral	**5**	**20**	**−44**	**57**	**44.85**
Postcentral	5	−24	−43	57	20.54
Precentral	6	20	−19	62	16.47
Medial frontal	6	4	−21	54	15.91
Insula	13	46	−32	24	15.54
Insula	13	−48	−28	17	14.03
Cuneus	18	−13	−82	21	11.16
Cuneus	18	12	−80	21	11.13
Middle occipital	37	38	−61	5	10.85

Coupling between Hubs and Networks

Across all 979 subjects and similarly to the single-subject analysis (see Supplementary Data), the coupling of the hubs

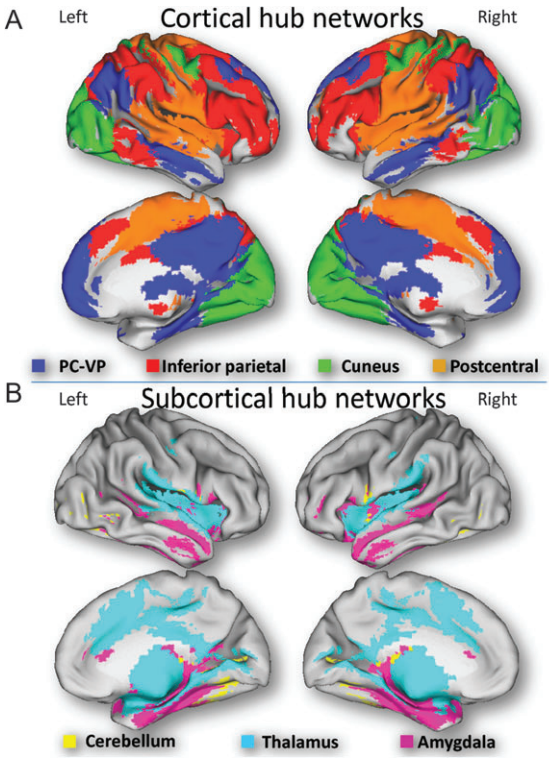

Figure 2. Cortical surface rendering. Overlays of cortical (*A*) and subcortical (*B*) hub networks on the inflated cerebral surface of the Human Colin template.

with their corresponding networks (diagonal correlation matrix elements; Fig. 5*A* left) was much stronger than with other networks (off diagonal elements) and the coupling between the PC-VP hub and the DMN was maximal. The resting-state activity in the cerebellum hub was significantly correlated with the average activity in the amygdala hub network. Similarly, the resting-state activity in the PC-VP hub was significantly anticorrelated with the average activity in the postcentral hub network. There was minimal coupling between hubs (elements of the upper triangular correlation matrix; Fig. 5*A* right panel) and a much stronger coupling between networks (elements of the lower triangular correlation matrix; Fig. 5*A* right panel). Specifically, the average signals in the subcortical hub networks (networks defined by hubs in cerebellum, thalamus, and amygdala) and the postcentral hub network were significantly correlated ($R > 0.3$), whereas the amygdala and cerebellum hub networks and the amygdala and postcentral hub networks showed the strongest positive coupling and the DMN and the postcentral hub network and the DMN and the cuneus hub network showed the strongest negative coupling (Fig. 5*B*).

Spectral Distribution of the Resting Brain Activity

The spectral distributions in Figure 6 show the 0.01–0.10 Hz low-frequency bandwidth of the average MRI signal time series across 979 subjects and imaging voxels for each of the 7 resting-state networks. While the analysis of single-subject data highlighted resonance frequencies that vary across subjects and imaging voxels (not shown), the average resting-state activity in each of the networks (Fig. 6*A*) did not show any resonance frequency and exhibited a monotonic decrease as a function of frequency that reflects the signal averaging across subjects and imaging voxels in the networks. The average power amplitude of the resting-state activity in the low-frequency bandwidth was highest for the DMN, consistently with previous studies (Zuo et al. 2010), and for the cuneus and thalamus hub networks and lowest for the cerebellum and amygdala hub networks (Fig. 6*B*).

Table 4
Statistical significance (*T*-score) of clusters functionally connected to the subcortical hubs (bolded) and their location in the Talairach stereotactic space

	BA/nucleus	*X*(mm)	*Y*(mm)	*Z*(mm)	*T*-score
Cerebellum hub network					
Cerebellum	**Fastigium**	**−9**	**−56**	**−20**	**49.56**
Hippocampus	Culmen	10	−56	−20	28.09
Subgyral		−23	−41	5	17.31
Parahippocampal	30	−23	−52	4	12.53
Insula	13	38	6	14	12.04
Insula	13	38	−3	18	11.92
Fusiform	37	−32	−60	−7	12.04
Lingual	19	−26	−63	−2	11.48
Posterior cingulate	29	−12	−47	10	11.74
Putamen	Lentiform	32	−4	2	11.35
Insula	13	−46	−5	14	11.23
Posterior cingulate	30	−24	−70	8	11.12
Insula	13	−32	0	15	11.08
Lingual	19	24	−72	3	10.68
Cuneus	17	18	−78	8	9.05
Insula	13	−32	−34	17	8.84
Posterior cingulate	29	−7	−42	14	8.52
Posterior cingulate	29	1	−37	17	8.33
Cingulate	24	4	−1	26	8.03
Postcentral	2	−38	−27	36	8.03
Postcentral	3	29	−31	45	8.01
Thalamus hub network					
Thalamus	**Medial dorsal**	**−12**	**−19**	**8**	**54.93**
Thalamus	Medial dorsal	7	−16	8	35.21
Lentiform nucleus	Putamen	−29	−18	−1	19.48
Cingulate gyrus	32	−1	12	38	19.15
Lingual gyrus	18	−1	−67	3	13.45
Lingual gyrus	18	−1	−80	−1	13.39
Lingual gyrus	18	10	−53	5	11.76
Superior temporal	22	−54	1	6	13.14
Cingulate gyrus	23	−1	−32	26	12.5
Cingulate gyrus	23	−1	−21	29	11.06
Precuneus	7	1	−39	44	12.14
Superior temporal	22	55	4	6	11.94
Superior temporal	22	−51	7	−1	11.59
Cerebellum	Culmen	−29	−55	−23	10.6
Cerebellum	Culmen	−20	−59	−21	10.27
Cerebellum	Declive	21	−62	−20	9.65
Cerebellum	Declive	7	−65	−15	9.05
Precentral	4	−40	−19	40	8.81
Precentral	4	37	−19	38	8.76
Cerebellum	Culmen	32	−53	−24	8.27
Postcentral	3	20	−33	58	8.16
"Reward-emotion" network					
Amygdala		**24**	**−6**	**−15**	**43.82**
Parahippocampal	36	27	−29	−9	14.93
Hippocampus		27	−35	1	13.9
Amygdala		−26	−8	−16	21.14
Hippocampus		−31	−28	−12	15.43
Hippocampus		−23	−35	−2	14.9
Midbrain	Mammillary	2	−9	−5	13.9
Midbrain	Red	2	−23	−14	13.8
Cingulate	24	−7	5	24	13.68
Cingulate	24	7	−7	28	13.57
Cingulate	24	12	−8	39	13.06
Superior temporal	38	44	5	−13	13.18
Superior temporal	38	−42	3	−15	13.05
Putamen	Lentiform	−23	6	15	12
Cingulate	24	−4	−7	25	12
Cingulate	31	18	−36	39	11.72
Thalamus	Pulvinar	−10	−28	18	11.72
Thalamus		2	−4	−1	11.27
Caudate		10	2	21	11.25
Insula	13	−37	−26	20	10.82
Cingulate	31	−13	−35	28	10.74
Postcentral	2	43	−24	27	10.5
Insula	13	38	22	15	10.25

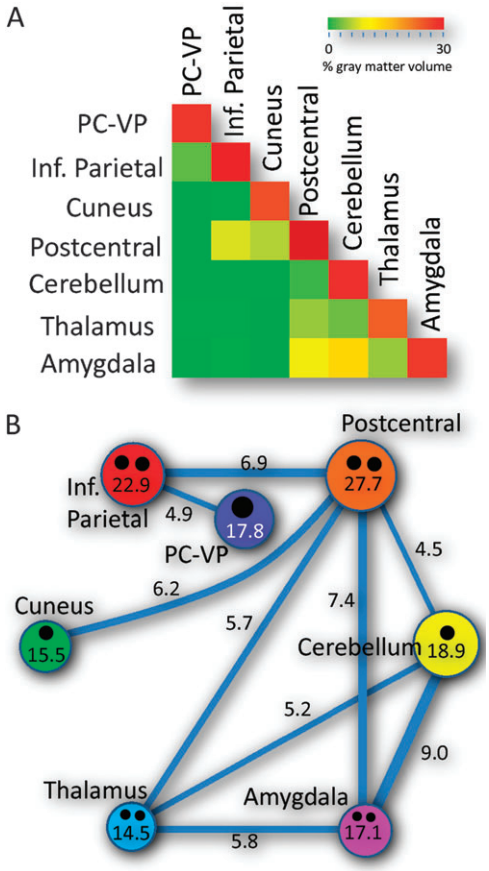

Figure 3. Network volumes and overlaps. (*A*) Triangular matrix showing the volume of the networks (main diagonal elements) and overlap between networks (off diagonal elements) for each the resting-state networks (circles) in Figure 1. (*B*) Diagram showing the overlap connection pattern (thickness of the connecting lines; numbers indicate percentage gray matter volume) and volume of the networks (areas of the color circles and numbers), as well and the number and strength (area of the black circles) of the network hubs (black circles). Volume threshold: 4.5% of the gray matter volume.

Scale-Free Topology of the Resting-State Hub Networks

Figure 7*A* shows for all 7 resting-state networks that the probability distribution, $P(k/k_0) = n(k/k_0)/n_0$, of the *l*FCD, decreased following the characteristic power law, $P(k/k_0) \propto (k/k_0)^{-\gamma}$, of the scale-free networks (Barabasi and Albert 1999; Barabasi 2009). Thus, in all resting-state networks, there were few intense hubs ($k/k_0 > 40$) and numerous weakly connected voxels ($k/k_0 < 10$). For illustration purposes, Figure 7*B* shows network diagrams with hypothetical central (high γ) and parallel (low γ) architectures. Whereas networks with high power scaling might have a central architecture with few strong hubs (large circles) and numerous weakly connected nodes (connections without circles), networks with low power scaling might have a parallel architecture with increased number of hubs and reduced number of weakly connected nodes. The power scale factor, γ (Fig. 7*A* bar graph insert), was significantly lower for the amygdala hub network and DAN (inferior parietal hub) than for the remaining networks ($P < 0.001$, comparison of regression slopes), whereas it was highest for the cuneus hub network. These findings indicate that the inferior parietal (cognition) and amygdala (emotion) hub networks favor more densely connected hubs with a differential balance between highly and weakly connected hubs that support a slightly more complex architecture in these networks.

Global Hubs Versus Local Hubs

The locations of the *g*FCD hubs were similar to those of the *l*FCD hubs. For both distributions, the PC-VP hub had the highest number of connections (Table 2). The strength of the rescaled *g*FCD was higher than that of the rescaled *l*FCD for the cerebellum. Conversely, the strength of the rescaled *g*FCD was lower than that of the rescaled *l*FCD for the remaining 6 hubs in this study. The analysis also revealed that for the PC-VP hub, the size of the *g*FCD cluster was much larger than that of the *l*FCD cluster and that the thalamus and cerebellum hubs were not identified by *g*FCD.

Discussion

Here, we present a functional connectivity approach for resting-state network mapping which does not require a priori anatomical selection for the seed locations. Instead we used FCDM (Tomasi and Volkow 2010), an ultrafast and data-driven approach for determining the regional density of functional connections, to identify the major cortical and subcortical functional connectivity hubs, which were then used as seed regions to map the functional networks of the resting state. We applied the method in 979 healthy humans from a large public database of resting state MRI time series (Biswal et al. 2010). Seven hubs were identified of 70 000 imaging voxels without a priori knowledge/hypotheses, which represents a 10^4-fold reduction in the complexity of the problem. Seven bilateral networks of the resting state of brain function emerged from the hub-voxel correlation analyses.

The PC-VP, the most connected functional hub in the brain, was functionally linked to the DMN (Raichle et al. 2001) that shows lower activity during goal-directed tasks than during resting baseline conditions (Fox et al. 2005; Tomasi et al. 2006). Since the DMN has been implicated in mind wandering (Mason et al. 2007), spontaneous cognition (Andrews-Hanna et al. 2010), and consciousness (Voss et al. 2006; Horovitz et al. 2009), we propose that the PC-VP hub performs information transfer and multimodal integration, which might be essential for processing spontaneous thoughts and internal awareness. This interpretation is consistent with studies reporting lower functional connectivity in DMN in neuropsychiatric diseases characterized by poverty of thought and disrupted states of consciousness such as schizophrenia, Alzheimer's disease, severe brain damage, and vegetative states (Voss et al. 2006; Buckner et al. 2008; Vanhaudenhuyse et al. 2010). The activity in the DMN was negatively correlated with the activity in the postcentral (somatosensory), cuneus (visual), cerebellum, and amygdala (emotional) hub networks (Fig. 5), which is consistent with prior studies reporting anticorrelated activity between the DMN and activated networks during task performance (Fox et al. 2005). Interestingly, the DMN had some overlap with the dorsal attention network but minimal overlap with the remaining networks (Fig. 3). This suggests an anatomical segregation of the DMN from the other networks, which might be necessary for its deactivation during task performance (Fox and Raichle 2007). The DMN along with the cuneus and thalamus hub networks showed the highest resting activity among the resting-state networks (Fig. 6), which is consistent with the default mode of human brain function

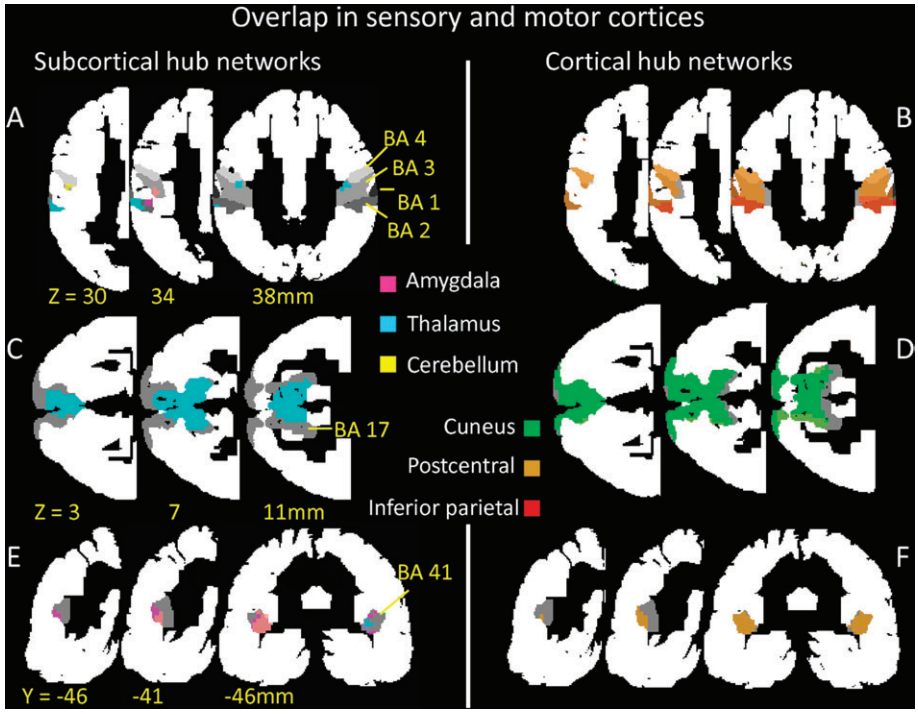

Figure 4. Network overlap in primary sensory and motor cortices. Overlap of subcortical (amygdala, thalamus, and cerebellum) and cortical (cuneus, postcentral, and inferior parietal) hub networks in primary somatosensory (BA 1–3) and motor (BA 4) (*A* and *B*), visual (BA 17; *C* and *D*), and auditory (BA 41; E and F) cortices (gray). Network overlap in other brain areas was masked out (white) using the Brodmann atlas included in the MRIcro software.

(Raichle et al. 2001; Raichle 2010) and might reflect the generation of spontaneous thoughts and internal awareness that occurs during resting conditions. Since glucose metabolism supports the energy requirements of neuronal activity (Shulman et al. 2001; Gruetter 2003; Raichle 2010) and it is assumed that the capacity of the human brain depends on energy-efficient cortical networks (Watts and Strogatz 1998; Laughlin and Sejnowski 2003; Salvador et al. 2005; Achard et al. 2006; Bassett and Bullmore 2006), our findings suggests that the higher glucose metabolism in regions of the DMN, as measured by 18F-fludeoxyglucose (FDG) positron emission tomography (PET) studies in resting conditions (Raichle and Gusnard 2002; Langbaum et al. 2009), serves to supports the higher communication rate of these regions. Due to its high resting activity and metabolic requirements, the DMN could be vulnerable to neurodegenerative disorders, as suggested by imaging studies on Alzheimer's disease (Buckner et al. 2009; Sperling et al. 2009).

The inferior parietal hubs were functionally connected to the DAN (Corbetta and Shulman 2002), which included frontal eye fields, ventral premotor cortex, prefrontal cortex, superior parietal lobule, intraparietal sulcus, motion-sensitive middle temporal areas, and thalamus. The DAN also included parts of the "control network" (dorsolateral and rostrolateral prefrontal, presupplementary motor area, inferior frontal junction, posterior parietal and premotor cortices, and the anterior insula), which is involved in cognitive control during task performance (Dosenbach et al. 2007). The DAN plays an important role in attention (Corbetta and Shulman 2002; Fan et al. 2005) and is implicated in alertness (Cavanna 2007), externally driven cognition, and working memory (Corbetta and Shulman 2002; Tomasi et al. 2007). The DAN showed minimal overlap with other networks and was the network that had the least correlated activity with other networks (Figs 3–5), suggesting that at rest the DAN is segregated from the other networks. The existence of 2 core hubs in the inferior parietal lobe suggests a parallel architecture for this network, which could facilitate focused attention. The DAN (together with the amygdala hub network) had the lowest fraction of weakly connected nodes and the highest fraction of highly connected hubs of the 7 resting networks (Fig. 7), which is consistent with a more complex architecture in this network. Even though the power amplitude of the signal fluctuations in the DAN was intermediate (Fig. 6), its high *f*FCD could make this network prone to dysfunction with the occurrence of brain metabolic deficits. Indeed, the high *f*FCD in the DAN could explain why attention and control deficits are at the core of neurocognitive deficits in Alzheimer's, Lewy body dementia, and vascular dementias (Fuentes et al. 2010; Luks et al. 2010).

The postcentral hub was functionally connected to the somatosensory network previously identified by early functional connectivity studies (Biswal et al. 1995; Xiong et al. 1999). This network had a high degree of integration (overlap and activity coupling) with all other resting-state networks (Figs 3–5). The postcentral hub network had extended connectivity with primary sensory and motor cortices (Fig. 4), which is consistent with the increased synchronization of neural activity in cortical regions during sensory processing (Srinivasan et al. 1999) and suggests an important role of the postcentral hub in conscious perception. The existence of mirror hubs (one in each brain hemisphere) in the somatosensory network suggests a stronger influence of the parallel architecture in this network. The somatosensory network and the DAN were the most extensive of the resting-state networks, covering 27% and 23% of the total gray matter in the brain.

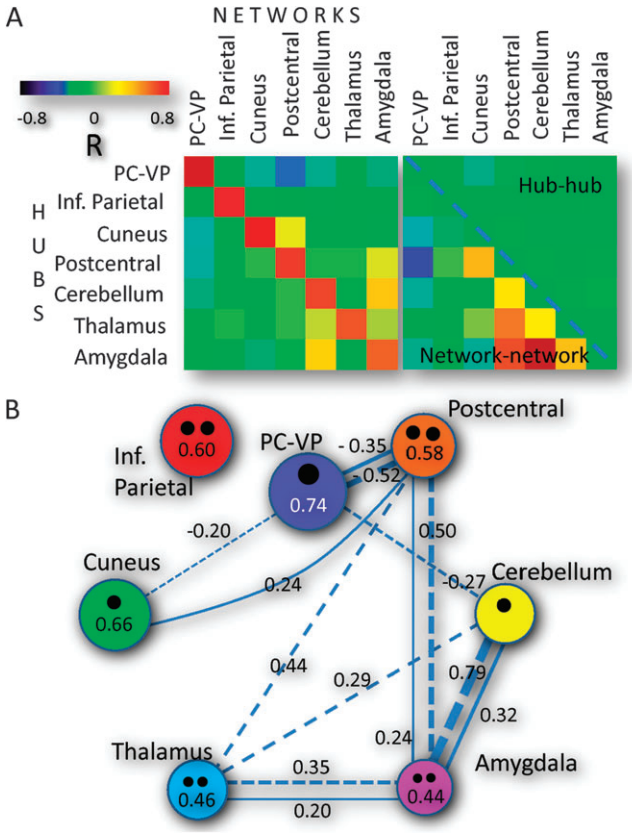

Figure 5. Network coupling across 979 subjects. (*A*) The hubs were strongly coupled with their associated networks (diagonal matrix elements) and weakly coupled with other networks (off diagonal elements) (Left). The coupling between hubs was minimal (elements of the upper triangular matrix) (Right). The couplings between the postcentral hub and subcortical networks and between the postcentral hub network and DMN (elements of the lower triangular matrix) were highly significant across subjects. (*B*) Diagram showing the correlation pattern between networks (thickness of the connecting dashed lines and closer numbers) and between hubs and their (area of color circles and numbers) and other (thickness of the connecting solid lines and closer numbers) networks as well and the number and strength (area of the black circles) of the network hubs (black circles). Correlation threshold: $|R| > 0.2$.

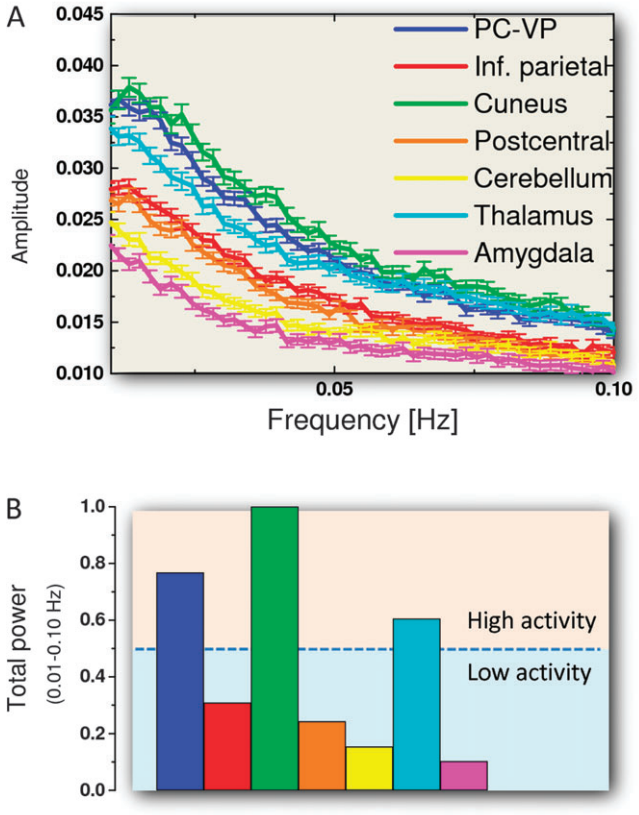

Figure 6. Spectral analysis. (*A*) Average spectral distribution of the spontaneous fluctuations of the brain activity across subjects and voxels for each of the resting-state networks (Figure 1) in the low-frequency bandwidth. Error bars are standard errors of the means. (*B*) Relative total power of the MRI spontaneous fluctuations in the low-frequency bandwidth (0.01–0.10 Hz). Three networks (PC-VP, cuneus, and thalamus) associated with consciousness, vision, and alertness had high resting activity (>50% of the maximum total power). Two of the subcortical networks (cerebellum and amygdala) had low resting activity.

The cuneus hub was functionally connected to a visual network that showed maximal power scaling (many weekly connected hubs and few densely connected hubs; Fig. 7). In fact, the multiple secondary hubs identified in this network (calcarine cortex, fusiform, lingual, and occipital gyri, and paracentral lobule) suggest a central architecture where the specialized visual processing performed by secondary hubs is integrated in the cuneus. This type of architecture may be necessary for the integration of visual information required for proper object identification. The cuneus hub network showed both correlated (with the somatosensory network) and anticorrelated (with DMN) activity with other networks. Thus, the visual network and the somatosensory network, which was also anticorrelated with DMN activity, may contribute to the anticorrelated activity reported between DMN and regions/networks activated by tasks that require visual and/or auditory processing (i.e., visual attention, target detection, reading, facial emotion recognition).

The cerebellar hub network comprised connections with most of the cerebellum, visual and limbic systems, parietal cortex, insula, and thalamus. The extended connectivity of the cerebellar network is consistent with recent findings linking the cerebellum with core networks involved in cognitive control (Habas et al. 2009), multiple cognitive operations (Schmahmann 1996), and emotions (Sacchetti et al. 2009). Note that the strong coupling between the cerebellar network and the other 2 subcortical networks (Fig. 5) might reflect the large overlap of the subcortical networks (Fig. 3) that might result from the higher contribution of short-range functional connections in cerebellum and thalamus. The low resting activity in the cerebellar network (Fig. 6) is consistent with the low metabolic rate of glucose reported by PET–FDG studies in this region (Kushner et al. 1987).

The thalamic hub network included the motor, premotor, visual, auditory, and limbic regions and the cerebellum in addition to the thalamus. This finding is consistent with the sensory gating function of the thalamus that acts as a relay between subcortical areas and the cerebral cortex (McCormick and Bal 1994; Tomasi et al. 2008) and the existence of massive thalamic projections to the ventral and dorsal premotor pathways in primates (Fang et al. 2006). The thalamus controls the flow of sensorimotor information to and from the cortex (McCormick and Bal 1994) and is a major processor of visual, auditory, and somatosensory information. The 2 major functional hubs were bilaterally located in the dorsal medial nuclei,

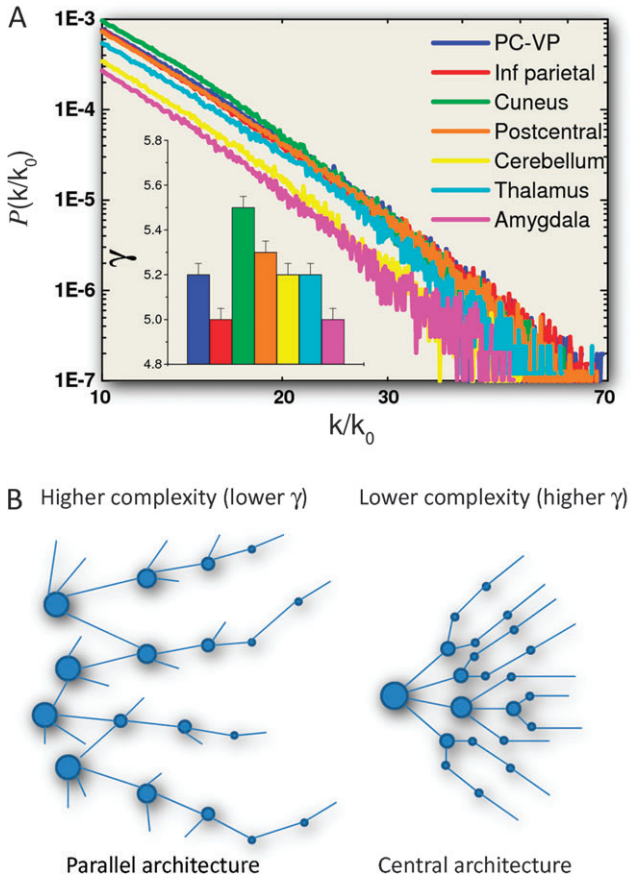

Figure 7. Power scaling. (*A*) Probability distribution of the FCD and power scaling factor, $-\gamma$, (bar plot insert) for each of the resting-state networks in Figure 1. Error bars reflect the standard errors of the means. (*B*) Diagrams showing hypothetical networks with extremely low (parallel architecture; left panel) and high (central architecture; right panel) power scaling factors. The area of the circles (hubs) represents the strength of the *l*FCD, and the connecting lines represent the functional connectivity between hubs and between hubs and weakly connected nodes.

which are essential for the alerting component of attention (Fan et al. 2005; Tomasi et al. 2009). These nuclei receive inputs from primary and secondary auditory cortices and are important for the detection of the relative intensity and duration of sounds. Thus, audiovisual sensory processing could partially explain the high activity of this network in resting conditions (Fig. 6). The thalamic network included regions from the "core network" (bilateral insula and the anterior cingulate cortex), which is believed to regulate transition from the default to the control mode of brain function (Dosenbach et al. 2007), and the auditory network (Damoiseaux et al. 2006). The minimal overlap (Fig. 3) and interaction (Fig. 5) between the thalamic network with the DAN supports the segregation of the alerting and orienting components of attention (Fan et al. 2005).

The amygdala hub network included the limbic system, midbrain, pons, striatum, lower thalamus, insula, as well as parietal and temporal cortices, regions that have been linked to reward and emotion (Murray 2007; Seymour and Dolan 2008; Colibazzi et al. 2010). The resting-state activity in this network was highly coupled with those of the cerebellum, thalamus, and postcentral hubs (Figs 3–5), and its average amplitude was the weakest among the 7 networks (Fig. 6), which could reflect the lack of reward/emotion modulations during resting-state MRI data acquisition.

Overall, the 7 resting networks detected using the major functional connectivity hubs (local maxima of *l*FCD) showed strong consistency with resting networks previously reported using arbitrary seed locations (Xiong et al. 1999; Beckmann et al. 2005; Damoiseaux et al. 2006; De Luca et al. 2006; van den Heuvel et al. 2009; Raichle 2010).

The *g*FCD mapping identified similar resting "functional hubs" in cortical regions as those obtained with *l*FCD, which indicates that these "functional hubs" have dense local as well as global connections. This also suggests that the functional networks identified with *l*FCD represent the basic organization of the resting brain. This postulate is also supported by the consistency between the networks we identified with *l*FCD and those previously reported using a priori "preselected" seed regions.

Different from *l*FDC, the analysis of the *g*FCD did not identify the thalamus and amygdala among the major "functional hubs," which suggests that these functional hubs have a predominance of local over global connections.

Study Limitations

In order to maximize reduction of complexity, we limited our approach to 7 brain regions (4 cortical and 3 subcortical); thus with only 7 hubs our method can capture up to 80% but not 100% of the gray matter. We did not include networks associated to other weaker hubs (i.e., caudate/orbitofrontal cortex), an approach that can increase the gray matter coverage, to minimize the complexity of the data. The participation of ventral frontal regions (orbitofrontal cortex) in the resting networks is underrepresented due to signal loss artifacts in fMRI with echo-planar imaging.

Conclusions

Using an ultrafast data-driven approach that can reduce the complexity of the data by a factor of 10^4 and resting-state data sets from 979 healthy humans, we identified the location of the major functional connectivity hubs in cortical and subcortical regions and the 7 bilateral networks, which cover 80% of the gray matter volume, that were associated to these hubs. The *g*FCD at the location of the cortical *l*FCD hubs was high suggesting that the long-range connectivity of the cortical hubs has an important role in network architecture. The most prominent functional hub was associated with the DMN, which had weak coupling (anticorrelated coupling with visual, somatosensory, and cerebellum networks) and minimal overlap with other networks (only with DAN). The segregation of the DMN and its maximal resting activity are consistent with its role in consciousness and its greater vulnerability for neurodegenerative diseases. All networks had a central architecture (few densely connected hubs and numerous weakly connected nodes) that is consistent with the scale-free topology but the scaling as well as the amplitude differed between the networks. The significant diversity among resting-state networks may influence their sensitivity/resilience to neuropathology.

Supplementary Material

Supplementary material can be found at: http://www.cercor.oxfordjournals.org/.

Funding

National Institutes of Alcohol Abuse and Alcoholism (2RO1AA09481).

Notes

Conflict of Interest: None declared.

References

Achard S, Salvador R, Whitcher B, Suckling J, Bullmore E. 2006. A resilient, low-frequency, small-world human brain functional network with highly connected association cortical hubs. J Neurosci. 26:63–72.

Andrews-Hanna JR, Reidler JS, Sepulcre J, Poulin R, Buckner RL. 2010. Functional-anatomic fractionation of the brain's default network. Neuron. 65:550–562.

Barabasi AL. 2009. Scale-free networks: a decade and beyond. Science. 325:412–413.

Barabasi AL, Albert R. 1999. Emergence of scaling in random networks. Science. 286:509–512.

Bassett DS, Bullmore E. 2006. Small-world brain networks. Neuroscientist. 12:512–523.

Beckmann CF, DeLuca M, Devlin JT, Smith SM. 2005. Investigations into resting-state connectivity using independent component analysis. Philos Trans R Soc Lond B Biol Sci. 360:1001–1013.

Biswal B, Yetkin FZ, Haughton VM, Hyde JS. 1995. Functional connectivity in the motor cortex of resting human brain using echo-planar MRI. Magn Reson Med. 34:537–541.

Biswal BB, Mennes M, Zuo XN, Gohel S, Kelly C, Smith SM, Beckmann CF, Adelstein JS, Buckner RL, Colcombe S, et al. 2010. Toward discovery science of human brain function. Proc Natl Acad Sci U S A. 107:4734–4739.

Buckner RL, Andrews-Hanna JR, Schacter DL. 2008. The brain's default network: anatomy, function, and relevance to disease. Ann N Y Acad Sci. 1124:1–38.

Buckner RL, Sepulcre J, Talukdar T, Krienen FM, Liu H, Hedden T, Andrews-Hanna JR, Sperling RA, Johnson KA. 2009. Cortical hubs revealed by intrinsic functional connectivity: mapping, assessment of stability, and relation to Alzheimer's disease. J Neurosci. 29:1860–1873.

Cavanna AE. 2007. The precuneus and consciousness. CNS Spectr. 12:545–552.

Colibazzi T, Posner J, Wang Z, Gorman D, Gerber A, Yu S, Zhu H, Kangarlu A, Duan Y, Russell JA, et al. 2010. Neural systems subserving valence and arousal during the experience of induced emotions. Emotion. 10:377–389.

Corbetta M, Shulman GL. 2002. Control of goal-directed and stimulus-driven attention in the brain. Nat Rev Neurosci. 3:201–215.

Cordes D, Haughton VM, Arfanakis K, Carew JD, Turski PA, Moritz CH, Quigley MA, Meyerand ME. 2001. Frequencies contributing to functional connectivity in the cerebral cortex in "resting-state" data. AJNR Am J Neuroradiol. 22:1326–1333.

Damoiseaux JS, Rombouts SA, Barkhof F, Scheltens P, Stam CJ, Smith SM, Beckmann CF. 2006. Consistent resting-state networks across healthy subjects. Proc Natl Acad Sci U S A. 103:13848–13853.

De Luca M, Beckmann CF, De Stefano N, Matthews PM, Smith SM. 2006. fMRI resting state networks define distinct modes of long-distance interactions in the human brain. Neuroimage. 29:1359–1367.

Dosenbach NU, Fair DA, Miezin FM, Cohen AL, Wenger KK, Dosenbach RA, Fox MD, Snyder AZ, Vincent JL, Raichle ME, et al. 2007. Distinct brain networks for adaptive and stable task control in humans. Proc Natl Acad Sci U S A. 104:11073–11078.

Fan J, McCandliss BD, Fossella J, Flombaum JI, Posner MI. 2005. The activation of attentional networks. Neuroimage. 26:471–479.

Fang PC, Stepniewska I, Kaas JH. 2006. The thalamic connections of motor, premotor, and prefrontal areas of cortex in a prosimian primate (Otolemur garnetti). Neurosci. 143:987–1020.

Foerster B, Tomasi D, Caparelli EC. 2005. Magnetic field shift due to mechanical vibration in functional magnetic resonance imaging. Magn Reson Med. 54:1261–1267.

Fox MD, Raichle ME. 2007. Spontaneous fluctuations in brain activity observed with functional magnetic resonance imaging. Nat Rev Neurosci. 8:700–711.

Fox MD, Snyder AZ, Vincent JL, Corbetta M, Van Essen DC, Raichle ME. 2005. The human brain is intrinsically organized into dynamic, anticorrelated functional networks. Proc Natl Acad Sci U S A. 102:9673–9678.

Friston K, Ashburner J, Kiebel S, Nichols T, Penny W. 2007. Statistical Parametric Mapping: the analysis of functional brain images. London: Academic Press.

Fuentes LJ, Fernández PJ, Campoy G, Antequera MM, García-Sevilla J, Antúnez C. 2010. Attention network functioning in patients with dementia with Lewy bodies and Alzheimer's disease. Dement Geriatr Cogn Disord. 29:139–145.

Gruetter R. 2003. Glycogen: the forgotten cerebral energy store. J Neurosci Res. 74:179–183.

Habas C, Kamdar N, Nguyen D, Prater K, Beckmann CF, Menon V, Greicius MD. 2009. Distinct cerebellar contributions to intrinsic connectivity networks. J Neurosci. 29:8586–8594.

He BJ, Zempel JM, Snyder AZ, Raichle ME. 2010. The temporal structures and functional significance of scale-free brain activity. Neuron. 66:353–369.

Horovitz SG, Braun AR, Carr WS, Picchioni D, Balkin TJ, Fukunaga M, Duyn JH. 2009. Decoupling of the brain's default mode network during deep sleep. Proc Natl Acad Sci U S A. 106:11376–11381.

Kushner M, Tobin M, Alavi A, Chawluk J, Rosen M, Fazekas F, Alavi J, Reivich M. 1987. Cerebellar glucose consumption in normal and pathologic states using fluorine-FDG and PET. J Nucl Med. 28:1667–1670.

Lancaster JL, Tordesillas-Gutiérrez D, Martinez M, Salinas F, Evans A, Zilles K, Mazziotta JC, Fox PT. 2007. Bias between MNI and Talairach coordinates analyzed using the ICBM-152 brain template. Human Brain Mapp. 28:1194–1205.

Lancaster JL, Woldorff MG, Parsons LM, Liotti M, Freitas CS, Rainey L, Kochunov PV, Nickerson D, Mikiten SA, Fox PT. 2000. Automated Talairach atlas labels for functional brain mapping. Hum Brain Mapp. 10:120–131.

Langbaum JB, Chen K, Lee W, Reschke C, Bandy D, Fleisher AS, Alexander GE, Foster NL, Weiner MW, Koeppe RA, et al. 2009. Alzheimer's disease neuroimaging initiative. Neuroimage. 45:1107–1116.

Laughlin SB, Sejnowski TJ. 2003. Communication in neuronal networks. Science. 301:1870–1874.

Luks TL, Oliveira M, Possin KL, Bird A, Miller BL, Weiner MW, Kramer JH. 2010. Atrophy in two attention networks is associated with performance on a Flanker task in neurodegenerative disease. Neuropsychologia. 48:165–170.

Mason MF, Norton MI, Van Horn JD, Wegner DM, Grafton ST, Macrae CN. 2007. Wandering minds: the default network and stimulus-independent thought. Science. 315:393–395.

McCormick DA, Bal T. 1994. Sensory gating mechanisms of the thalamus. Curr Opin Neurobiol. 4:550–556.

Murray EA. 2007. The amygdala, reward and emotion. Trends Cogn Sci. 11:489–497.

Raichle ME, Gusnard DA. 2002. Appraising the brain's energy budget. Proc Nat Acad Sci U S A. 99:10237–10239.

Raichle ME. 2010. Two views of brain function. Trends Cogn Sci. 14:180–190.

Raichle ME, MacLeod AM, Snyder AZ, Powers WJ, Gusnard DA. 2001. A default mode of brain function. Proc Natl Acad Sci U S A. 98:676–682.

Sacchetti B, Scelfo B, Strata P. 2009. Cerebellum and emotional behavior. Neuroscience. 162:756–762.

Salvador R, Suckling J, Coleman MR, Pickard JD, Menon D, Bullmore E. 2005. Neurophysiological architecture of functional magnetic resonance images of human brain. Cereb Cortex. 15:1332–1342.

Schmahmann JD. 1996. From movement to thought: anatomic substrates of the cerebellar contribution to cognitive processing. Hum Brain Mapp. 4:174–198.

Seeley WW, Crawford RK, Zhou J, Miller BL, Greicius MD. 2009. Neurodegenerative diseases target large-scale human brain networks. Neuron. 62:42–52.
Seymour B, Dolan R. 2008. Emotion, decision making, and the amygdala. Neuron. 58:662–671.
Shulman GL, Corbetta M, Fiez JA, Buckner RL, Miezin FM, Raichle ME, Petersen SE. 1997. Searching for activations that generalize over tasks. Hum Brain Mapp. 5:317–322.
Shulman RG, Hyder F, Rothman DL. 2001. Lactate efflux and the neuroenergetic basis of brain function. NMR Biomed. 14:389–396.
Sperling RA, Laviolette PS, O'Keefe K, O'Brien J, Rentz DM, Pihlajamaki M, Marshall G, Hyman BT, Selkoe DJ, Hedden T, et al. 2009. Amyloid deposition is associated with impaired default network function in older persons without dementia. Neuron. 63:178–188.
Srinivasan R, Russell DP, Edelman GM, Tononi G. 1999. Increased synchronization of neuromagnetic responses during conscious perception. J Neurosci. 19:5435–5448.
Tomasi D, Caparelli EC. 2007. Macrovascular contribution in activation patterns of working memory. J Cereb Blood Flow Metab. 27:33–42.
Tomasi D, Chang L, Caparelli EC, Ernst T. 2007. Different activation patterns for working memory load and visual attention load. Brain Res. 1132:158–165.
Tomasi D, Chang L, Caparelli EC, Ernst T. 2008. Sex differences in sensory gating of the thalamus during auditory interference of visual attention tasks. Neurosci. 151:1006–1015.
Tomasi D, Ernst T, Caparelli EC, Chang L. 2006. Common deactivation patterns during working memory and visual attention tasks: an intra-subject fMRI study at 4 Tesla. Hum Brain Mapp. 27:694–705.
Tomasi D, Volkow ND. 2010. Functional connectivity density mapping. Proc Natl Acad Sci U S A. 107:9885–9890.
Tomasi D, Wang RL, Telang F, Boronikolas V, Jayne MC, Wang GJ, Fowler JS, Volkow ND. 2009. Impairment of attentional networks after 1 night of sleep deprivation. Cereb Cortex. 19:233–240.
Tzourio-Mazoyer N, Landeau B, Papathanassiou D, Crivello F, Etard ODelcroix N, Mazoyer B, Joliot M. 2002. Automated anatomical labeling of activations in SPM using a macroscopic anatomical parcellation of the MNI MRI single-subject brain. Neuroimage. 15:273–289.
van den Heuvel MP, Mandl RC, Kahn RS, Hulshoff Pol HE. 2009. Functionally linked resting-state networks reflect the underlying structural connectivity architecture of the human brain. Hum Brain Mapp. 30:3127–3141.
van den Heuvel MP, Stam CJ, Boersma M, Hulshoff Pol HE. 2008. Small-world and scale-free organization of voxel-based resting-state functional connectivity in the human brain. Neuroimage. 43:528–539.
Vanhaudenhuyse A, Noirhomme Q, Tshibanda LJ, Bruno MA, Boveroux P, Schnakers C, Soddu A, Perlbarg V, Ledoux D, Brichant JF, et al. 2010. Default network connectivity reflects the level of consciousness in non-communicative brain-damaged patients. Brain. 133:161–171.
Voss HU, Uluç AM, Dyke JP, Watts R, Kobylarz EJ, McCandliss BD, Heier LA, Beattie BJ, Hamacher KA, Vallabhajosula S, et al. 2006. Possible axonal regrowth in late recovery from the minimally conscious state. J Clin Invest. 116:2005–2011.
Watts DJ, Strogatz SH. 1998. Collective dynamics of 'small-world' networks. Nature. 393:440–442.
Xiong J, Parsons LM, Gao JH, Fox PT. 1999. Interregional connectivity to primary motor cortex revealed using MRI resting state images. Hum Brain Mapp. 8:151–156.
Zuo XN, Di Martino A, Kelly C, Shehzad ZE, Gee DG, Klein DF, Castellanos FX, Biswal BB, Milham MP. 2010. The oscillating brain: complex and reliable. Neuroimage. 49:1432–1445.